Method to account for the effect of hydrodynamics on polar organic compound uptake by passive samplers

Kees Booij*, Natasja L. Maarsen, Matthijs Theeuwen, Ronald van Bommel

NIOZ Royal Netherlands Institute for Sea Research, P.O. Box 59, 1790 AB Texel, The Netherlands

* Corresponding author, present address: PaSOC, Greate Pierwei 25, 8821 LV Kimswerd, The Netherlands,

T. +31 517 234 174, E. keesbooij@pasoc.eu

Address correspondence to keesbooij@pasoc.eu

Abstract

Mass transfer coefficients of the water boundary layer (k_w) were measured using alabaster dissolution kinetics in a diffusion cell that was operated at stirring rates between 90 and 600 min^{-1}, aiming to provide a more robust characterisation of the effect of hydrodynamics on the uptake of polar compounds by passive samplers, as compared with characterisations in terms of stirring rates and water flow velocities. The measured k_w helped to quantitatively understand calcium sulphate transport through a poly(ethersulfone) membrane and two water boundary layers (at both sides of the membrane). Alabaster based k_w were used to understand atrazine transport in the diffusion cell, allowing the conclusion that atrazine transport in the membrane is via the pore space, rather than via the polymer matrix. The merits of measuring alabaster dissolution rates for passive sampler calibration and application in the field is discussed. We propose that passive sampler calibrations be carried out under controlled k_w conditions, rather than under controlled stirring rates or flow velocities. This would facilitate the interpretation of passive sampler calibration studies and the translation of laboratory based water sampling rates to flow conditions that apply in the field.

Key words: Analytical chemistry, Organic contaminants, Passive sampler, Calibration, Water boundary layer, Mass transfer

Running head: Accounting for hydrodynamics in passive sampling

INTRODUCTION

Passive samplers of polar organic chemicals are frequently used for monitoring concentration levels of these compounds in environmental waters. These samplers include the polar organic chemical integrative sampler (POCIS) [1], the polar version of the Chemcatcher [2], the cellulose/iso-octane/dodecanol sampling device (CIDS) [3], and the diffusive gradients in thin films for organics (o-DGT) [4], among others. These devices typically consist of a sorption phase that is covered by a microporous membrane made of poly(ethersulfone) (PES) or poly(sulfone) for POCIS and Chemcatcher, cellulose for CIDS, or an overlay of agarose gel and PES for o-DGT. Commonly used sorption phases are granular poly(divinylbenzene-*co*-*N*-vinylpyrrolidone) or a mixture of sorbents (activated carbon - poly(styrene-*co*-divinylbenzene) - polystyrene) for POCIS, poly(styrene-co-divinylbenzene) for Chemcatchers, granular poly(divinylbenzene-*co*-*N*-vinylpyrrolidone) suspended in agarose gel for o-DGT, or a mixture of 1-dodecanol and 2,2,4-trimethylpentane for CIDS. Chemicals of interest diffuse from bulk water through the water boundary layer (WBL), into the membrane, and further into the sorption phase. Despite their apparent simplicity, our knowledge of mass transport towards and within these samplers is rather limited. Harman et al. [5] reviewed the calibration and use of POCIS and concluded that the effect of water flow velocity, temperature, pH, ionic strength, biofouling, and compound properties on the uptake rates by POCIS are poorly understood, and that mechanistic models are needed to increase our understanding of this sampler.

The common approach to calibrate the uptake kinetics of polar compounds by passive samplers is to expose the samplers to contaminated water and to monitor the depletion rate of the water [6,7] and/or the accumulation rate of the sampler [8–10]. Flow conditions are reported sometimes as average flow velocities (*U*) at some distance from the sampler surface [9,11–13], and sometimes as stirring rates of a magnetic or overhead stirring device [4,8]. In other studies, flow is qualitatively characterized as "turbulent" or "quiescent" [1,14]. Uptake rates of many polar chemicals are often found to be higher at higher flow rates, but it is difficult to apply this observation to field-exposed samplers, because stirring rates obtained in the laboratory and qualitative characteristics like "turbulent" versus "quiescent" cannot be easily linked to flow velocities in the field. In addition, these characterizations of water flow do not provide a sound basis for developing mechanistic models for passive sampler - water exchange. The options for the use of average flow velocities in passive sampler calibration studies are better, but some challenges exist. First, it is not always clear from the literature reports if *U* was calculated (e.g., from pumping rates and cross-sectional areas of the exposure system), or measured using a current meter. Second, uptake rates may also depend on the direction of the flow relative to the sampler surface and on the turbulence intensity, which may both be different in the field and in the laboratory.

Mass transport rates can be conveniently parameterised using mass transfer coefficients (MTCs), which are the proportionality constants (k_i) between the steady state flux (j_i - amount per unit surface area per unit time) through a phase i and the concentration difference over this phase (ΔC_i)

$$j_i = k_i \ \Delta C_i \qquad (1)$$

Uptake of chemicals by passive samplers involves transport through the WBL, through the membrane, and into the sorption phase, where each transport step can be characterized by an MTC, if steady state conditions apply. Under the assumption that the MTCs are independent of time, and that local sorption equilibrium exists at the interfaces, the relative importance of mass transport through the WBL, the membrane and the sorption phase can be evaluated from [15–17]

$$\frac{1}{k_o} = \frac{1}{k_w} + \frac{1}{k_m K_{mw}} + \frac{1}{k_s K_{sw}} \quad (2)$$

where K_{mw}, is the membrane-water partition coefficient of the chemical of interest, K_{sw} is its sorbent-water partition coefficient, k_w, k_m, k_s are the MTCs of the WBL, the membrane and the sorption phase, and k_o is the overall MTC that relates the flux to the effective concentration difference between water and sorbent.

$$j = k_o\left(C_w - \frac{C_s}{K_{sw}}\right) \quad (3)$$

In passive sampling research it is common practice to express compound accumulation as an equivalent water sampling rate (R_s), which is related to k_o by

$$R_s = k_o A \quad (4)$$

where A is the surface area of the sampler. Hence, k_o can be interpreted as a surface area normalised sampling rate, with units of L dm^{-2} d^{-1} or μm s^{-1}, for example.

Equation 2 expresses that the overall transport resistance ($1/k_o$) equals the sum of the transport resistances of the WBL, the membrane and the sorption phase. In studies on uptake rates by the diffusive gradients in thin films sampler (DGT) it was shown that plotting the overall transport resistance as a function of the membrane thickness allowed estimation of the WBL resistance [18–20], and below we demonstrate that manipulation of the WBL resistance allows to measure the membrane resistance, using a similar approach.

The use of MTCs is convenient, because they can often be experimentally determined and require no knowledge of transport mechanisms on the molecular level or the structure of the membrane. A limitation is that their use relies on the assumption that they are independent of time, which is not always the case at the initial stages of passive sampler exposures [21,22]. In addition, transport within the sorption compartment can be expected to be fairly complicated due to the existence of different pore space domains, nonlinear sorption isotherms, and the mixed occurrence of

absorption by the sorbent polymer and adsorption to the polymer surface [23]. Still, equation 2 may be a valuable tool to gain more insight into the mechanisms of solute transfer to passive samplers because it allows for separating the effects of transport through the WBL, the membrane, and the sorbent. For example, the product $k_m K_{mw}$ can be experimentally determined in membrane permeation experiments (i.e., without a sorbent) by measuring k_o at known values of k_w. The obtained value may in turn be used to evaluate the sorbent term ($k_s K_{sw}$) by studying the k_o of solute uptake by intact passive samplers as a function of k_w. Equation 2 also provides a basis for comparing laboratory calibration studies for passive samplers, because it allows for separating the effects of flow, which are exposure specific, and the effects of sampler layout and compound properties. Knowledge of the value of k_w is therefore crucial in this respect.

A number of methods exist for estimating k_w. Stephens et al. [24] adopted an equation for mass transfer to a flat plate under laminar flow

$$k_w = 0.664 \frac{D_w}{L} \left(\frac{\nu}{D_w} \right)^{1/3} \left(\frac{UL}{\nu} \right)^{1/2} \quad (5)$$

where D_w is the diffusion coefficient in water, ν is the kinematic viscosity of water, U is the flow velocity, and L is the length of the plate. Taking L to be the sampler diameter, these authors could predict the sampling rates of four polar compounds by C18 and sulfonated poly(styrene-*co*-divinylbenzene) extraction disks within a factor of 2, assuming that the uptake was fully WBL controlled. Adopting a length scale L = 10 cm, and $D_w = 5 \cdot 10^{-10}$ m^2 s^{-1}, equation 5 predicts k_w values between 1 and 60 μm s^{-1}, at flow velocities between 0.05 and 200 cm s^{-1}. A similar range of k_w values (1 - 50 μm s^{-1}) was suggested by Lohmann [25]. Experimental values of k_w can be obtained by measuring the limiting current for some electrochemical reactions (e.g., reduction of hexacyanoferrate(III)) on an electrode surface [26–28], or by studying the dissolution kinetics of benzoic acid that is coated on the surface of interest [29–31].

115 The alabaster dissolution rate method is an alternative method for obtaining k_w in the laboratory
116 and in the field [32–34]. Alabaster is a natural deposit of gypsum ($CaSO_4 \cdot 2H_2O$), which can be purchased
117 from sculpture supply shops. The method relies on the assumption that the dissolution process is rate
118 limited by transport through the WBL, rather than by solvation from the crystal lattice. The evolution of
119 the mass loss (Δm) of a dissolving alabaster plate is then given by

120 $$\Delta m = VC_w^* \left[1 - \exp\left(-\frac{k_w A t}{V} \right) \right] \quad (6)$$

121 where C_w^* is the alabaster solubility (mass per volume units), V is the water volume, t is time, and A is the
122 surface area of the plate. Rearranging equation 6 yields k_w as a function of the observed mass loss

123 $$k_w = -\frac{V}{At} \ln\left(1 - \frac{\Delta m}{VC_w^*} \right) \quad (7)$$

124 For k_w measurements in the field (i.e., very large water volumes), equation 7 reduces to

125 $$V \to \infty : \; k_w = \frac{\Delta m}{AtC_w^*} \quad (8)$$

126 since ln(1-x) $\to$ -x when x $\to$ 0. It should be noted that C_w^* is the alabaster solubility in the exposure
127 medium, i.e., background concentrations of calcium and sulphate should be taken into account [35].

128 For the present study we chose to assess the merits of alabaster dissolution rate measurements
129 by also studying the mass transfer rates in a diffusion cell that consisted of two stirred compartments
130 with equal volume (V), which were separated by a PES membrane with surface area A.

131 With identical hydrodynamic conditions at both sides of the membrane, k_o is given by

132 $$\frac{1}{k_o} = \frac{2}{k_w} + \frac{1}{k_m K_{mw}} \quad (9)$$

133 The factor 2 in equation 9 emerges because in this system there is a WBL at both sides of the membrane.
134 Plotting $1/k_o$ as a function of $1/k_w$ (as determined from the alabaster dissolution method) then should
135 yield a straight line with slope 2 and intercept $1/(k_m K_{mw})$.

When the background concentrations in both compartments equal zero, the evolution of concentrations in the donor compartment (C_1) and the acceptor department (C_2) is given by

$$C_1 = \frac{C_0}{2}\left[1 + \exp\left(-\frac{2k_o A t}{V}\right)\right] \quad (10)$$

$$C_2 = \frac{C_0}{2}\left[1 - \exp\left(-\frac{2k_o A t}{V}\right)\right] \quad (11)$$

where C_0 is the concentration in the donor compartment at $t = 0$. Estimates of k_o and C_0 can be obtained by curve fitting of equations 10 and 11 to all experimental C_1 and C_2 data. Alternatively, these parameters can be obtained for each individual sampling time by elimination:

$$C_0 = C_1 + C_2 \quad (12)$$

$$k_o = -\frac{V}{2At}\ln\left(\frac{C_1 - C_2}{C_1 + C_2}\right) \quad (13)$$

The purpose of the present work was to assess the performance of the alabaster dissolution rate method for calibrating the hydrodynamics of calibration setups for passive samplers of polar chemicals. This method was chosen because it can also be applied for passive sampler exposures in the environment. Membrane permeation experiments were carried out to check consistency with the alabaster dissolution measurements.

METHODS

Diffusion cell

The diffusion cell was made of 6 mm thick polyacrylate, and consisted of two 1-L compartments that were separated by an impermeable wall with a 5 cm wide opening, in which a membrane or an alabaster plate could be mounted (Supplemental Data, S1). The diameter of the exposed alabaster and membrane surface was 4.0 cm. Both cells were stirred with an overhead stirrer (IKA RW20) with speed detector and regulator. The 4-blade (2.5 × 1.0 cm) stirring shaft was positioned 5 mm above the bottom.

The effect of stirrer height on the k_o of sodium chloride at 400 min^{-1} was found to be insignificant (CV=3% for six stirrer heights in the range 3-20 mm above the bottom). The diffusion cell was placed in a temperature controlled water bath. Experiments were carried out at a temperature of 21.0 ± 1.5 °C. Poly(ethersulfone) membranes (PAL Life sciences, Supor-200, 47 mm diameter, 145 μm nominal thickness, 0.2 μm nominal pore size) were conditioned overnight in demineralised water before use.

Chemicals

KCl (Sigma-Aldrich, ACS reagent) was pre-combusted 16 h at 500 °C. NaCl (BDH, AnalaR NORMAPUR) and CaSO4·2H_2O (Merck, MSURE) were used as received. White, translucent, alabaster was purchased from a local sculpture supplies shop, and was shaped into 1 cm thick, 4 cm diameter slices that were pre-weighted and mounted in a poly(oxymethylene) holder that was clamped vertically in the compartment separation wall (Supplemental Data, S1).

Conductivity measurements

Electrolyte concentrations were determined using a Greisinger GMH3430 conductivity meter. The cell constant was calibrated using 0.01 and 0.1 m KCl solutions [36]. Calibration functions were obtained by fitting measured conductivities (κ) to the electrolyte's concentration (5-12 levels over the range 0.01- 1 g L^{-1}) according to

$$\kappa - \kappa_0 = aC - b\,C^{3/2} + d\,C^2 \quad (14)$$

where κ_0 is the background conductivity of the deionized water after equilibration with atmospheric CO_2 and *a*, *b*, *d* are fitting parameters. Calibration solutions were prepared by mass (g kg^{-1} solution). Concentrations were converted to g L^{-1} using solution densities that were calculated from the apparent molar volumes and the Redlich-Meyer limiting slopes at 25 °C, as outlined by Millero [37]. Solution densities of the most concentrated solutions (2.5 g L^{-1} $CaSO_4$·2H_2O) were only 0.2% higher than those of pure water, indicating that the effect of dissolved electrolytes on the solution density can be neglected

for future studies. Because the inverse function of equation 14 is not easily obtained, experimental concentrations were obtained recursively from

$$C_{i+1} = \frac{\kappa - \kappa_0}{a - b\sqrt{C_i} + d\,C_i} \quad (15)$$

where new estimates of the concentration (C_{i+1}) were calculated from previous values (C_i) until a constant value was obtained (Supplemental Data, S2).

Permeation experiments

Permeation experiments with electrolytes were conducted by filling both compartments with equal masses of deionized water, followed by a 30-min period to allow atmospheric CO_2 to equilibrate with the water. At t = 0, a spike solution in water was added to the donor compartment and an equal water mass was added simultaneously to the receptor compartment. Conductivities were measured at 5 min time intervals during the first hour, followed by a 30 -60 min intervals (during office hours). Concentrations were chosen so as to obtain a conductivity just below 200 μS cm^{-1} in the donor compartment, in order to have all conductivity readings on the same scale of the instrument. Control experiments were carried out before and after each permeation experiment, as a check on equipment failure (e.g., membrane rupture, leaking O-ring). These experiments involved monitoring the permeation of a 1 g L^{-1} NaCl solution for 1 h at fixed times at a stirring rate of 400 min^{-1}. The k_o for these control experiments showed a coefficient of variation of 3%, and corrective measures were taken when k_o deviated more than 9% from the average (replacement of the membrane or the O-ring).

Permeation rates of atrazine were studied by spiking a water volume of 1040 mL with 36 ng mL^{-1} atrazine. This spiked water and an equal volume of ultrapure water were added simultaneously to the compartments. Six to eight water samples (10 mL) were taken to monitor the evolution of concentrations over a time period of 55 to 160 h. After addition of internal standard (110 ng atrazine-d5) the water samples were extracted using solid phase extraction columns filled with 0.2 g Oasis HLB on a

vacuum manifold (Baker SPE-12G), followed by drying under vacuum (~ 20 min). Columns were eluted with methanol. Extracts were evaporated to dryness under a stream of nitrogen, and the residue was redissolved in 50 μL ethyl-acetate. After addition of an injection internal standard (50 μL anthracene-d10 solution in 2,2,4-trimethylpentane) the samples were analysed by GC/MS in selective ion monitoring mode (m/z = 200 and 205).

Alabaster solubility and dissolution rates

Alabaster solubility was determined by incubating pre-weighed alabaster pieces (size ~2 cm) in 200 mL water in a closed glass vessel for 24 h under continuous stirring (400 min^{-1}), at temperatures of 4 and 20 °C, and NaCl background concentrations of 0 and approximately 36 g kg^{-1}. Solubilities of pure $CaSO_4 \cdot 2H_2O$ were calculated as outlined elsewhere [35].

MTCs of the WBL were measured by mounting a pre-weighed alabaster plate (40 mm diameter and ~ 1 cm thickness) in the wall of one of the compartments (Supplemental Data, S1). The position of the alabaster surface was the same as the position of the membrane during the permeation experiments. Alabaster mass losses were determined after drying the plates at 60 °C for 30 min, followed by cooling in ambient air. Mass loss rates ranged from about 30 - 300 mg h^{-1} at stirring rates between 0 and 600 min^{-1}.

At very high mass transfer rates, the solvation of ions from the crystal lattice may become rate limiting. To investigate this, two experiments were carried out, in which an alabaster plate was positioned under a tap water jet that hit the surface at a right angle, with velocities of 3 and 8 m s^{-1}.

Hydraulic permeability

The hydraulic permeability of the membranes was determined by filling both compartments of the diffusion cell to just above the top of the membrane (850 mL) followed by the addition of 350 mL water to one compartment, and monitoring the water levels in both compartments over time. Hydraulic

permeation was modelled using Darcy's law, which relates the water flux through the membrane (q = volume change per unit surface area and unit time) to the pressure difference (Δp) over the membrane

$$q = -\frac{k}{\mu}\frac{\Delta p}{d} = -K\frac{\Delta h}{d} \quad (16)$$

where μ is the dynamic viscosity of the water, d is the membrane thickness (145 μm), k is the permeability of the membrane (m^2), and $K = k\rho g/\mu$ is the hydraulic conductivity ($m\ s^{-1}$), with ρ the density of the water and g the acceleration of gravity. The difference in water levels (Δh) is then governed by

$$\Delta h = \Delta h_0 \exp\left(-\frac{2 K A_m}{d A_s} t\right) \quad (17)$$

where t is time, Δh_0 is the water level difference at $t = 0$, A_m is the surface area of the membrane (12.6 cm^2), and A_s is the cross sectional area of the compartments (1.1 dm^2).

RESULTS AND DISCUSSION

Alabaster dissolution

Experimental alabaster solubilities were in good agreement with the values that were calculated from O'Brien et al. [35]. Ratios of measured/calculated solubilities (1.028 ± 0.016, n = 6) showed no systematic trend with temperature (4 and 21 °C) or NaCl background concentrations (0 and 36 g kg^{-1}) (Supplemental Data, S3). The slightly higher experimental solubilities may be related to the presence of water soluble impurities that were co-precipitated during alabaster deposition. Although the correction factor is rather close to 1, it may be higher or lower for other alabaster batches, depending on the deposit.

Measured k_w increased from 2.7 μm s^{-1} at 0 min^{-1} to 27 μm s^{-1} at 600 min^{-1} (Figure 1). Method repeatability was about 6% at stirring rates of 200, 400, and 600 min^{-1} (two experimenters, n = 3 for each stirring rate) and 12% at 0 min^{-1} (one experimenter, n = 4) (Supplemental Data, S4). Between 90 and 600

248 min^{-1}, k_w increased with stirring rate to the power 0.74, but attained a value of 2.7 ± 0.3 μm s^{-1} in the
249 absence of forced convection (Figure 1 and Supplemental Data, S4).

250 The nonzero value of k_w under unstirred conditions may be explained by the free convection
251 currents that result from the greater density of the saturated calcium sulphate solution near the
252 alabaster surface, relative to the density of the bulk water (~ 0.0021 g cm^{-3} difference). The observed k_w
253 is close to the value of 3.0 μm s^{-1} that is calculated from the Churchill-Chu equation for free convection
254 heat and mass transfer near vertical plates (Supplemental Data, S5). Incropera et al. [38] proposed to
255 model the effect of free convection on the total MTC by

256 $$(k_w)^n = (k_{w,free})^n \pm (k_{w,forced})^n \quad (18)$$

257 where the minus sign applies for opposing flows (forced flow opposite to the direction of free
258 convection) and the plus sign applies for assisting and transverse flows, and n = 3 to 4. Adopting a
259 conservative value of n = 3, the effect of free convection on k_w is estimated to be less than 10% when k_w
260 is larger than 1.5 times $k_{w,free}$, indicating that this method is limited to the measurement of k_w values
261 larger than 4 μm s^{-1}.

262 The highest dissolution rates were obtained for the experiments in which an alabaster plate was
263 positioned under a tap water jet that hit the surface at a right angle, with velocities of 3 and 8 m s^{-1}. The
264 resulting k_w's (120 and 300 μm s^{-1}, respectively) gave no reason to believe that solvation kinetics was a
265 rate limiting factor at the stirring rates that were used.

266 *Electrolyte permeation*

267 The permeation experiments were carried out to investigate if alabaster dissolution rate
268 measurements help to understand mass transfer through membranes and (ultimately) mass transfer to
269 passive samplers. At the initial stages of this study, the overall MTCs (k_o) of calcium sulphate were
270 estimated from equations 10 and 11 using nonlinear least squares, but it was observed that the residual
271 errors showed systematic deviations (Supplemental Data, S6). The high accuracy of the conductivity

measurements allowed k_o to be estimated for individual points in time (equation 13). In most cases, k_o increased with time during the first half day, after which it attained a constant value (Figure 2), although one occurrence of decreasing values was also observed. We have no definite explanation for the cause of this effect, but we speculate that it is related to an initial difference in hydrostatic pressure between the compartments that induces a water flow across the membrane. As time goes by, this water flow causes the pressure difference to decrease, which in turn causes the flow to fade out. Results of the hydraulic permeation experiments indicated that differences in water height decrease with a first order rate constant of 0.36 h^{-1}, which corresponds to a hydraulic conductivity of K = 0.060 μm s^{-1} (Supplemental Data, S7). This implies that an initially 1 mm higher water level in the acceptor compartment generates a 0.43 μm s^{-1} water flow into the donor compartment, and hence reduces k_o by the same value. The initial values of k_o were on average 0.25 μm s^{-1} smaller than the plateau value (range 0.14 to 0.42 μm s^{-1}), which can then be explained by assuming a 0.6 mm difference in water level. This difference may be caused by a slight tilt of the diffusion cell support, by small asymmetries in the dimensions of the two compartments, or by the volume of the conductivity sensor (3 to 10 cm^3, depending on the immersion depth). The results of the hydraulic permeation experiments indicated that water level equilibration takes place with half-life time of 2 h, which is in accordance with the time needed for k_o to attain a constant value (Figure 2). We therefore adopted the plateau values (t > 24 h) as the best available estimates of k_o. The relative standard deviations of these plateau values ranged from 0.1 to 0.8%. Permeation experiments at 90 and 400 min^{-1} were carried out in duplicate, and differences between the duplicates were 2.0 and 3.5%, respectively.

Increasing the stirring rate from 90 to 600 min^{-1} causes an increase of k_o by a factor of 1.7 (Figure 3). The conductivity of the membrane ($k_m K_{mw}$) for calcium sulphate transport can be estimated from the measured values of k_o and k_w by

$$\frac{1}{k_m K_{mw}} = \frac{1}{k_o} - \frac{2}{k_w} \quad (19)$$

which yielded a value of 4.3 ± 0.3 μm s^{-1}. It may appear in Figure 3 that the membrane conductivity is higher (4.6 μm s^{-1}) at 90 min^{-1}, but it should be noted that the accuracy of this estimate is lower than at higher stirring rates. For example, an error in k_o and k_w of 5% results in an error in $k_m K_{mw}$ of 13% at 90 min^{-1} and 7% at 600 min^{-1}, while all estimates deviated less than 10% from the average.

A more insightful visualisation of the data can be obtained by plotting the overall transport resistance ($1/k_o$) as a function of the WBL resistance ($1/k_w$), as shown in Figure 4. In this case, there is a mechanistic relationship between the dependent variable ($1/k_o$) and independent variable ($1/k_w$) via equation 19, in contrast with the representation in Figure 3, where the relationship with the independent variable (stirring rate) is empirical.

The expectation value of $k_m K_{mw}$ for solutes that are only transported via the water filled pores of the membrane can be estimated from the mass transport equations for porous media [39]

$$k_m K_{mw} = \frac{\phi D_w}{d\ \tau^2} \quad (20)$$

where ϕ is the porosity, d is the membrane thickness and τ is the tortuosity (length of the diffusion path divided by the thickness of the membrane; some authors use the name "tortuosity factor" for τ^2). Adopting ϕ = 0.7, D_w= 800 $\mu m^2\ s^{-1}$, d = 145 μm, and τ = 1 yields a value of $k_m K_{mw}$ = 3.9 μm s^{-1}, which is 11% smaller than the experimental value of 4.3 ± 0.3 μm s^{-1}. In the absence of accurate values for ϕ and τ this can be considered to be a satisfactory correspondence. It should also be noted that the manufacturer lists a "typical thickness" of 145 μm for PES membranes with a nominal pore size of 0.2 μm, and specifies that the actual thickness could range between 130 and 163 μm. This means that a specific membrane could have a thickness that is 10% lower or 12% higher than the nominal thickness.

Atrazine permeation

Overall MTCs of atrazine were estimated by nonlinear least squares regression (equations 10 and 11), and ranged from 1.3 μm s^{-1} at 90 min^{-1} to 2.3 μm s^{-1} at 600 min^{-1}. Recoveries were 83 ± 8 % (estimated C_0 relative to the concentration that was calculated from the spiked amount). Residual errors were about 0.6 ng mL^{-1} (~ 4% of the average concentrations). Atrazine amounts detected in the membrane were 1.0 ± 0.5 % of the amounts in the water (n = 6), which yields a tentative PES-water sorption coefficient of 130 L kg^{-1}. Experiments at 90, 400, and 600 min^{-1} were repeated 3 months later by a second experimenter, who obtained k_o estimates that were 8 - 22 % lower. A data summary is given in the Supplemental Data (S4).

The k_w obtained from alabaster dissolution can be used for other compounds after accounting for differences in diffusion coefficient. Although exact k_w - D_w relationships are only available for a limited number of flow configurations, it is widely accepted to take k_w to be proportional to the 2/3 power of the diffusion coefficient [24,40–43]. It then follows that the k_w of compound i ($k_{w,i}$) can be estimated from the alabaster based value ($k_{w,CaSO4}$) and the respective diffusion coefficients ($D_{w,i}$ and $D_{w,CaSO4}$) from

$$k_{w,i} = k_{w,CaSO4}\left(\frac{D_{w,i}}{D_{w,CaSO4}}\right)^{2/3} \quad (21)$$

The aqueous diffusion coefficient of atrazine is reported to be 560 μm^2 s^{-1} at 20 °C [44]. With $D_{w,CaSO4}$ = 800 μm^2 s^{-1} this implies that the k_w of atrazine is a factor of 1.26 lower than the k_w of calcium sulphate. Values of 1/ k_o for atrazine permeation increase linearly with 1/ k_w with a slope of 2 and an intercept 1/($k_m K_{mw}$), in accordance with equation 9 (Figure 5).

The membrane conductivity ($k_m K_{mw}$) obtained by experimenter 1 was 3.2 μm s^{-1}. The standard error of the mean (SEM) was 0.26 μm s^{-1} (n = 4). Estimates of $k_m K_{mw}$ from experimenter 2 were lower (2.5 μm s^{-1}) and showed a smaller scatter (SEM : 0.07 μm s^{-1}, n = 4). Experimental values were 19% higher (experimenter 1) and 7% lower (experimenter 2) than the theoretical value obtained from equation 20

(adopting ϕ = 0.7, D_w= 560 μm^2 s^{-1}, d = 145 μm, and τ = 1), which can be considered to be a satisfactory agreement. Transport through the polymer matrix cannot be completely excluded, but is not likely to be important, in view of the low PES-water sorption coefficients and the fact that the membrane conductivity was in good agreement with equation 20 .

The data from this experiment suggest that atrazine transport through the PES membrane is through the pore space, rather than through the polymer matrix. But more importantly, this approach allows to assess data quality through the uncertainty in the intercept of $1/k_o$ vs. $1/k_w$ and through the deviation of individual measurements from the theoretical slope. Such assessments are not possible when empirical relationships between sampling rates and flow rates or stirring rates are used.

IMPLICATIONS FOR PASSIVE SAMPLING CALIBRATION AND APPLICATION

The present study demonstrates the merits of measuring k_w using alabaster dissolution rates for quantifying the mass transfer resistance of PES membranes, albeit for one organic compound only. Yet, we expect that this method may also be used to improve our understanding of the uptake rates of polar organic compounds by passive samplers for several reasons. First, this method allows to separate the effects of flow from the effects of membrane and sorption phase on the uptake rates. This facilitates comparability of passive sampler calibrations between laboratories, because flow conditions are laboratory specific, while the transport resistances of membrane and sorbent are sampler/compound specific. Second, the quantification of k_w may help strengthening the theoretical framework for interpreting sampling rates. Presently reported sampling rates are often difficult to interpret in terms of transport resistances of the WBL, the membrane, and the sorbent, because these sampling rates reflect the combined effects of transport through all of these phases. It can be expected that improved knowledge of the importance of the separate transport steps helps to improve passive sampler design. Improved mechanistic understanding of the uptake kinetics is also much needed for estimating the

363 uncertainties in passive sampler based monitoring, which in turn is indispensable for the application of
364 passive samplers in a regulatory context. Third, the alabaster dissolution rate method may help in
365 translating the results of laboratory calibrations to field conditions. Laboratory calibrations obtained
366 under defined stirring rates are obviously difficult to apply in the field. But also the use of (measured)
367 flow velocities has it difficulties, because exposures in laboratory and field may differ in the
368 presence/absence of protective cages and in the angle of incidence of the incoming water. More robust
369 sampling rate estimates for field exposures may be obtained through equation 2, by combining the WBL
370 resistance that is measured in the field, with compound/sampler specific transport resistances of
371 membrane and sorption phase that are obtained in the laboratory. This improvement can be achieved
372 with relatively little effort, because quantification of k_w requires the determination of a mass loss of a
373 few hundred milligrams, which can be achieved after a 1 to 5 hour exposure time, depending on the
374 flow.

375 A number of caveats for the proposed method should be mentioned as well. First, this method is
376 limited to the measurement of k_w values > 4 μm s^{-1} (flow velocities > 2.4 cm s^{-1}, based on equation 5)
377 because free convection currents that are generated by the alabaster dissolution itself cannot be
378 neglected at lower values. An alternative could be to obtain k_w from the dissipation of performance
379 reference compounds from nonpolar passive samplers, provided that the sampler-water partition
380 coefficients (including their temperature dependence) are as accurately known as the solubility of
381 calcium sulphate. This is a challenge on its own. Calibrating the dissipation kinetics from nonpolar
382 passive samplers against the dissolution kinetics of alabaster may permit the quantification of k_w values <
383 4 μm s^{-1}. Second, alabaster solubility is a critical parameter in the k_w measurement, which is close to, but
384 likely always different from the solubility of pure calcium sulphate. The solubility of alabaster should
385 therefore be calibrated against the literature values for each new batch of alabaster, preferably at
386 different temperatures, as outlined above. Third, when applying this method in connection with passive

samplers, the membrane/sorbent envelope of sub-millimetre thickness is replaced by an alabaster plate of 4-10 mm thickness. This may have an effect on the hydrodynamical conditions at the alabaster surface, and some additional experiments may be needed to investigate the effect of plate thickness on k_w. Forth, upper and lower limits exist for the permissible alabaster exposure time. The mass loss should be sufficiently large to be measured accurately. After exploring various drying techniques we selected drying for 30 min at 60 ^oC, followed by cooling in ambient air. This procedure yielded a precision of about 1 mg for 4 cm diameter plates. We therefore recommend a minimum mass loss of 200 mg for this plate diameter. For the upper mass loss limit, it should be considered that the alabaster surface recedes as a result of the dissolution process and may become increasingly shielded from the flow. We suggest a maximum mass loss of 1.5 g for a 4 cm diameter plate, which corresponds to a surface recession of 0.5 mm. However, a smaller mass loss in the range 200-400 mg is sufficiently accurate and extends the life time of the plate.

Summarising, the measurement of k_w using dissolution rates of flat alabaster plates is not a full solution for all flow related challenges with passive sampler calibration and application, but may be helpful for strengthening the mechanistic basis of models for polar compound uptake by passive samplers.

Supplemental Data - The Supplemental Data are available on the Wiley Online Library

Acknowledgment - We thank Joanne Beerda and Hamidreza Sharifan for their participation in this study.

Data availability - The raw data are provided in the Supplemental Data.

409 # REFERENCES

410 1. Alvarez DA, Petty JD, Huckins JN, Jones-Lepp T, Getting DT, Goddard J, Manahan SE. 2004.
411 Development of a passive, in situ, integrative sampler for hydrophilic organic contaminants in
412 aquatic environments. *Environ.Toxicol.Chem.* 23:1640–1648.
413 2. Kingston JK, Greenwood R, Mills GA, Morrison GM, Persson LB. 2000. Development of a novel
414 passive sampling system for the time-averaged measurement of a range of organic pollutants in
415 aquatic environments. *J.Environ.Monit.* 2:487–495.
416 3. Hyne RV, Aistrope M. 2008. Calibration and field application of a solvent-based cellulose membrane
417 passive sampling device for the monitoring of polar herbicides. *Chemosphere*. 71:611–620.
418 4. Chen CE, Zhang H, Jones KC. 2012. A novel passive water sampler for in situ sampling of antibiotics.
419 *J.Environ.Monit.* 14:1523–1530.
420 5. Harman C, Allan IJ, Vermeirssen ELM. 2012. Calibration and use of the polar organic chemical
421 integrative sampler - a critical review. *Environ.Toxicol.Chem.* 31:2724–2738.
422 6. Li HX, Helm PA, Metcalfe CD. 2010. Sampling in the Great Lakes for pharmaceuticals, personal care
423 products, and endocrine-disrupting substances using the passive polar organic chemical integrative
424 sampler. *Environ.Toxicol.Chem.* 29:751–762.
425 7. Macleod SL, McClure EL, Wong CS. 2007. Laboratory calibration and field deployment of the polar
426 organic chemical integrative sampler for pharmaceuticals and personal care products in wastewater
427 and surface water. *Environ.Toxicol.Chem.* 26:2517–2529.
428 8. Belles A, Tapie N, Pardon P, Budzinski H. 2014. Development of the performance reference
429 compound approach for the calibration of 'polar organic chemical integrative sampler' (POCIS).
430 *Anal.Bioanal.Chem.* 406:1131–1140.

9. Li HX, Vermeirssen ELM, Helm PA, Metcalfe CD. 2010. Controlled field evaluation of water flow rate effects on sampling polar organic compounds using polar organic chemical integrative samplers. *Environ.Toxicol.Chem.* 29:2461–2469.
10. Lissalde S, Mazzella N, Fauvelle V, Delmas F, Mazellier P, Legube B. 2011. Liquid chromatography coupled with tandem mass spectrometry method for thirty-three pesticides in natural water and comparison of performance between classical solid phase extraction and passive sampling approaches. *J.Chromatogr.A*. 1218:1492–1502.
11. Kaserzon SL, Hawker DW, Booij K, O'Brien DS, Kennedy K, Vermeirssen ELM, Mueller JF. 2014. Passive sampling of perfluorinated chemicals in water: In-situ calibration. *Environ.Pollut.* 186:98–103.
12. Mazzella N, Lissalde S, Moreira S, Delmas F, Mazellier P, Huckins JN. 2010. Evaluation of the use of performance reference compounds in an Oasis-HLB adsorbent based passive sampler for improving water concentration estimates of polar herbicides in freshwater. *Environ.Sci.Technol.* 44:1713–1719.
13. Vermeirssen ELM, Dietschweiler C, Escher BI, van der Voet J, Hollender J. 2012. Transfer kinetics of polar organic compounds over polyethersulfone membranes in the passive samplers POCIS and Chemcatcher. *Environ.Sci.Technol.* 46:6759–6766.
14. Martinez Bueno MJ, Hernando MD, Aguera A, Fernandez-Alba AR. 2009. Application of passive sampling devices for screening of micro-pollutants in marine aquaculture using LC-MS/MS. *Talanta*. 77:1518–1527.
15. Flynn GL, Yalkowsky SH. 1972. Correlation and prediction of mass transport across membranes I: Influence of alkyl chain length on flux-determining properties of barrier and diffusant. *J.Pharm.Sci.* 61:838–852.
16. Huckins JN, Petty JD, Booij K. 2006. *Monitors of organic chemicals in the environment: semipermeable membrane devices.* Springer, New York.

17. Vrana B, Popp P, Paschke A, Schuurmann G. 2001. Membrane-enclosed sorptive coating. An integrative passive sampler for monitoring organic contaminants in water. *Anal.Chem.* 73:5191–5200.
18. Chen CE, Zhang H, Ying GG, Jones KC. 2013. Evidence and recommendations to support the use of a novel passive water sampler to quantify antibiotics in wastewaters. *Environ.Sci.Technol.* 47:13587–13593.
19. Garmo OA, Royset O, Steinnes E, Flaten TP. 2003. Performance study of diffusive gradients in thin films for 55 elements. *Anal.Chem.* 75:3573–3580.
20. Zhang H, Davison W. 1995. Performance characteristics of diffusion gradients in thin films for the in situ measurement of trace metals in aqueous solution. *Anal.Chem.* 67:3391–3400.
21. Booij K, Vrana B, Huckins JN. 2007. Chapter 7, Theory, modelling and calibration of passive samplers used in water monitoring. In Greenwood, R, Mills, GA and Vrana, B, eds, *Passive sampling techniques in environmental monitoring*. Elsevier, pp 141–169. Available from http://dx.doi.org/10.1016/S0166-526X(06)48007-7.
22. Tcaciuc AP, Apell JN, Gschwend PM. 2015. Modeling the transport of organic chemicals between polyethylene passive samplers and water in finite and infinite bath conditions. *Environ.Toxicol.Chem.* 34:2739–2749.
23. Gorecki T, Yu XM, Pawliszyn J. 1999. Theory of analyte extraction by selected porous polymer SPME fibres. *Analyst*. 124:643–649.
24. Stephens BS, Kapernick A, Eaglesham G, Mueller J. 2005. Aquatic passive sampling of herbicides on naked particle loaded membranes: Accelerated measurement and empirical estimation of kinetic parameters. *Environ.Sci.Technol.* 39:8891–8897.

25. Lohmann R. 2012. Critical review of low-density polyethylene's partitioning and diffusion coefficients for trace organic contaminants and implications for its use as a passive sampler. *Environ.Sci.Technol.* 46:606–618.
26. Beck RE, Schultz JS. 1972. Hindrance of solute diffusion within membranes as measured with microporous membranes of known pore geometry. *Biochim.Biophys.Acta*. 255:273–303.
27. Rodrigues C, Geraldes V, de Pinho MN, Semião V. 2012. Mass-transfer entrance effects in narrow rectangular channels with ribbed walls or mesh-type spacers. *Chem.Eng.Sci.* 78:38–45.
28. Szanto DA, Cleghorn S, Ponce-De-Len C, Walsh FC. 2008. The limiting current for reduction of ferricyanide ion at nickel: The importance of experimental conditions. *AICHE J.* 54:802–810.
29. Garner FH, Grafton RW. 1954. Mass transfer in fluid flow from a solid sphere. *Proc.R.Soc.Lond.A.Math.Phys.Sci.* 224:64–82.
30. Irandoust S, Andersson B. 1986. Concentration-dependent diffusivity of benzoic acid in water and its influence on the liquid–solid mass transfer. *Can.J.Chem.Eng.* 64:954–959.
31. Mao HH, Chisti Y, Moo-Young M. 1992. Multiphase hydrodynamics and solid-liquid mass transport in an external-loop airlift reactor - a comparative study. *Chem.Eng.Commun.* 113:1–13.
32. Opdyke BN, Gust G, Ledwell JR. 1987. Mass transfer from smooth alabaster surfaces in turbulent flows. *Geophys.Res.Lett.* 14:1131–1134.
33. Santschi PH, Anderson RF, Fleisher MQ, Bowles W. 1991. Measurements of diffusive sublayer thicknesses in the ocean by alabaster dissolution, and their implications for the measurements of benthic fluxes. *J.Geophys.Res.-Oceans*. 96:10641–10657.
34. Santschi PH, Bower P, Nyfeller UP, Azevedo A, Broecker WS. 1983. Estimates of the resistance to chemical transport posed by the deep-sea boundary layer. *Limnol.Oceanogr.* 28:899–912.
35. O'Brien DS, Booij K, Hawker DW, Mueller JF. 2011. Method for the in situ calibration of a passive phosphate sampler in estuarine and marine waters. *Environ.Sci.Technol.* 45:2871–2877.

501 36. Pratt KW., Koch WF, Wu YC, Berezansky PA. 2001. Molality-based primary standards of electrolytic
502 conductivity. *Pure Appl.Chem*. 73:1783–1793.
503 37. Millero FJ. 1972. The partial molal volumes of electrolytes in aqueous solutions. In Horne, RA, ed.,
504 *Water and aqueous solutions. Stucture, thermodynamics, and transport processes.* John Wiley and
505 Sons, New York, pp 519–564.
506 38. Incropera FP, Bergman TL, Lavine AS, DeWitt DP. 2015. *Fundamentals of heat and mass transfer.* 7th,
507 John Wiley & Sons, Hoboken, N.J.
508 39. Epstein N. 1989. On tortuosity and the tortuosity factor in flow and diffusion through porous media.
509 *Chem.Eng.Sci.* 44:777–779.
510 40. Bohrer MP. 1983. Diffusional boundary layer resistance for membrane transport.
511 *Ind.Eng.Chem.Fund.* 22:72–78.
512 41. Deen WM, Bohrer MP, Epstein NB. 1981. Effects of molecular-size and configuration on diffusion in
513 microporous membranes. *AICHE J.* 27:952–959.
514 42. Knudsen JG, Hottel HC, Sarofim AF, Wankat PC, Knaebel KS. 1999. Heat and mass transfer. In Green,
515 DW and Maloney, JO, eds, *Perry's Chemical Engineers' Handbook. 7th Ed.* McGraw-Hill, New York.
516 43. Levich VG. 1962. *Physicochemical hydrodynamics.* Prentice Hall, Inc., Englewood Cliffs, NJ.
517 44. Calvet R. 1976. Mesure rapide du coefficient de diffusion de l'atrazine en solution aqueuse. *Weed*
518 *Res.* 16:53–55.
519

Figures

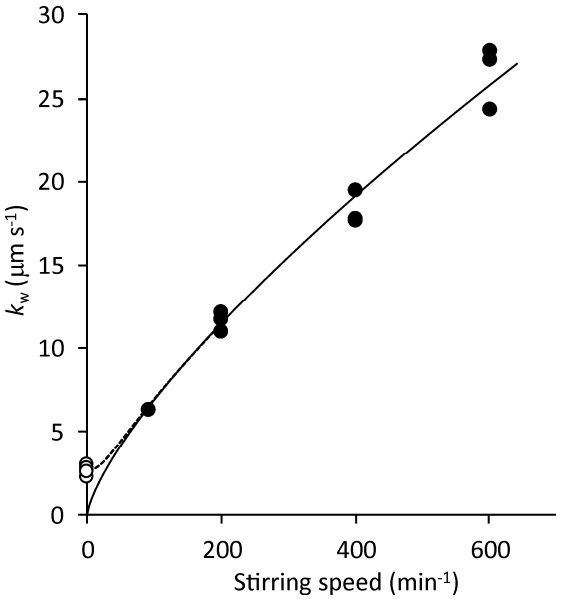

Figure 1. Mass transfer coefficients (k_w) of the water boundary layer obtained from alabaster dissolution rates as a function of stirring speed (f) at 0 min^{-1} (open circles) and 90 to 600 min^{-1} (filled circles). The drawn line represents the forced convection component ($k_w = 0.23\, f^{0.74}$), and equation 18 is shown as a dashed line.

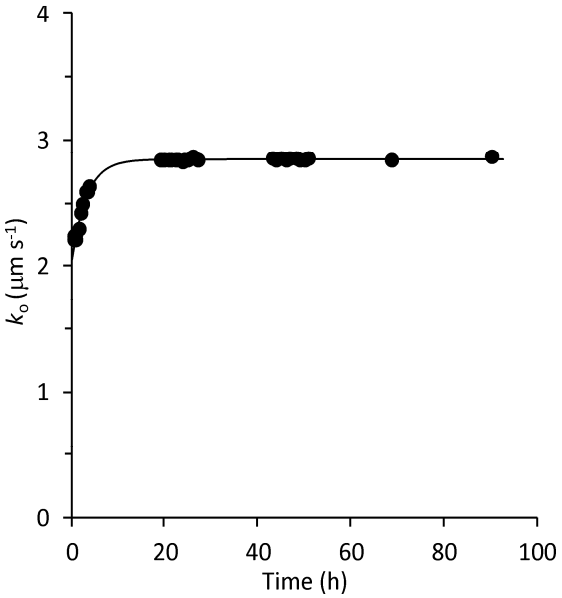

Figure 2. Time dependency of the overall mass transfer coefficient (k_o) of calcium sulphate for a permeation experiment at a stirring rate of 400 min^{-1}. The drawn line is shown as a guide for the eye.

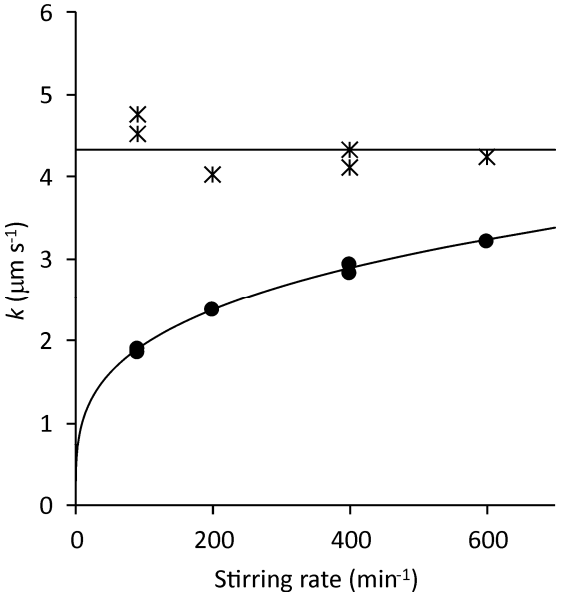

Figure 3. Overall mass transfer coefficients (k_o) for calcium sulphate permeation (circles) and estimates of $k_m K_{mw}$ (asterisks) as a function of stirring rate. The horizontal line represents the average $k_m K_{mw}$. The curved line ($k_o = 0.53\, f^{0.28}$) is shown as a guide for the eye.

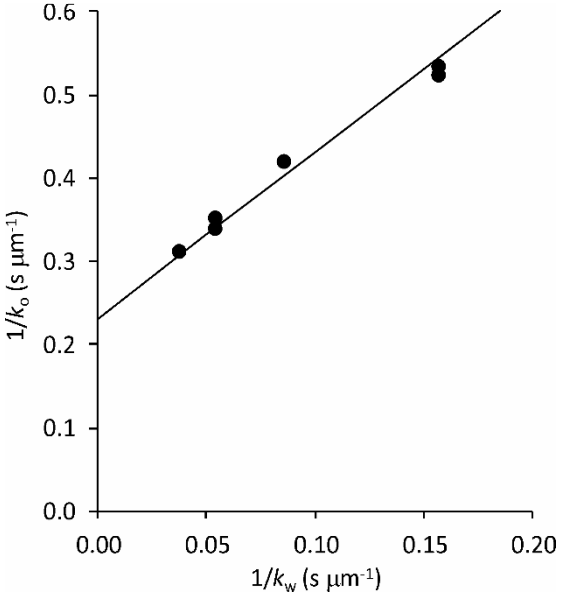

Figure 4. Overall mass transfer resistance ($1/k_o$) for calcium sulphate permeation. The drawn line represents the model equation $1/k_o = 1/(k_m K_{mw}) + 2/k_w$.

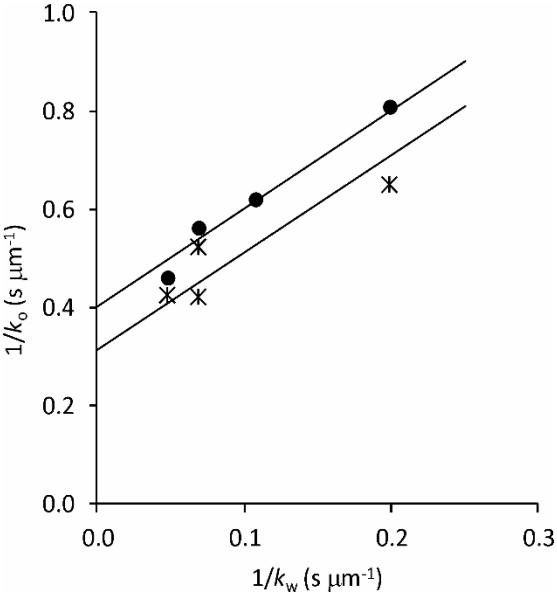

536

537 **Figure 5.** Overall mass transfer resistance ($1/k_o$) for atrazine permeation measured by experimenters 1

538 (asterisks) and 2 (circles). The drawn lines represent the model equation $1/k_o = 1/(k_m K_{mw}) + 2/k_w$.

Supplemental data

Method to account for the effect of hydrodynamics on polar organic compound uptake by passive samplers

Kees Booij* , Natasja L. Maarsen, Matthijs Theeuwen, Ronald van Bommel

NIOZ Royal Netherlands Institute for Sea Research, P.O. Box 59, 1790 AB Texel, The Netherlands
* Corresponding author, present address: PaSOC, Greate Pierwei 25, 8821 LV Kimswerd, The Netherlands

S1 Diagram of the experimental setup

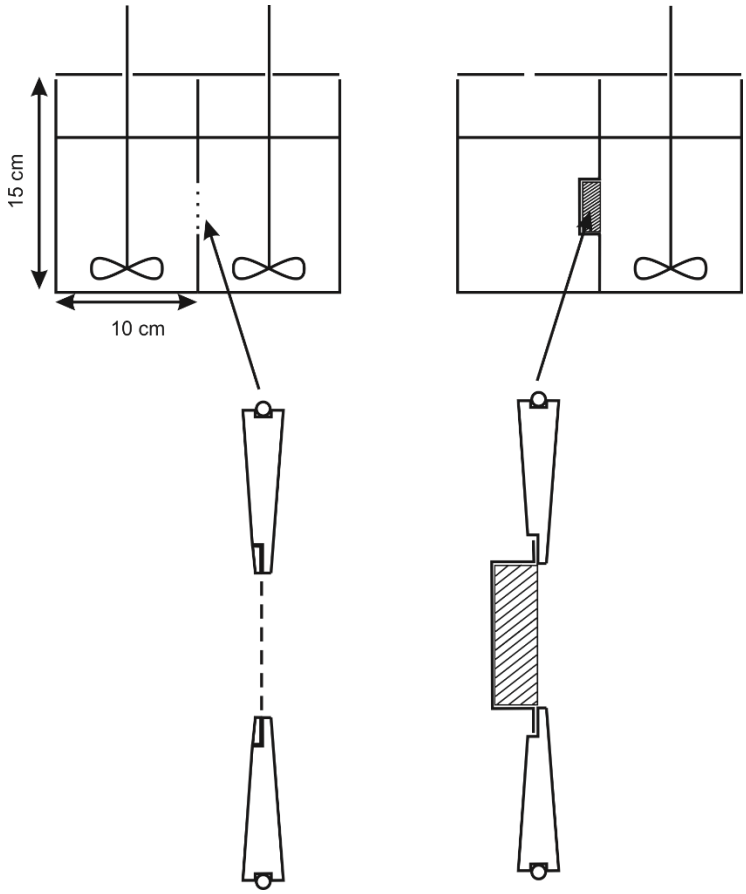

Figure S1-1. Schematic drawing of the setup for measuring permeation rates (left) and alabaster dissolution rates (right): overview (top) and expanded view of the opening in the separation wall between the compartments (bottom).

S2 Calculation of electrolyte concentrations from conductivity

The conductivity (κ) of the electrolyte solutions was modelled as a function of concentration using

$$\kappa - \kappa_0 = aC - b\,C^{3/2} + dC^2 \qquad \text{(S2-1)}$$

Because the inverse of this equation is not readily available, eq. S2-1 was rearranged to

$$C = \frac{\kappa - \kappa_0}{a - b\,C^{1/2} + dC} \qquad \text{(S2-2)}$$

A first estimate of C can be obtained by setting $C = 0$ at the right hand side of eq. S2-2

$$C_{i=1} = \frac{\kappa - \kappa_0}{a} \qquad \text{(S2-3)}$$

This value is used at the right hand side of eq. S2-2 to obtain a better estimate of C

$$C_{i=2} = \frac{\kappa - \kappa_0}{a - b\,C_{i=1}{}^{1/2} + d\,C_{i=1}} \qquad \text{(S2-4)}$$

This process is repeated until the change in subsequent concentration estimates is sufficiently small.

Below follows a sample calculation.
During one of the permeation experiments with calcium sulphate, the conductivity reading was 192.0 μS cm^{-1}, and the conductivity-concentration relationship was

$$\kappa = 0.80 + 1448.3\, C - 738.6\, C^{3/2} + 193.1\, C^2 \qquad \text{(S2-5)}$$

with κ in μS cm^{-1} and C in g L^{-1}. From eq. S2-3, the first concentration estimate is

$$C_{i=1} = \frac{\kappa - \kappa_0}{a} = \frac{192.0 - 0.8}{1448.3} = 0.1320 \ \text{g L}^{-1} \qquad \text{(S2-6)}$$

Subsequently better estimates are obtained from eq S2-4

$$\begin{aligned} C_{i=2} &= \frac{192.00 - 0.80}{1448.3 - 138.6 \times (0.1320)^{1/2} + 193.1 \times 0.1320} = 0.1586 \ \text{g L}^{-1} \\ C_{i=3} &= \frac{192.00 - 0.80}{1448.3 - 138.6 \times (0.1586)^{1/2} + 193.1 \times 0.1586} = 0.1614 \ \text{g L}^{-1} \\ C_{i=4} &= \frac{192.00 - 0.80}{1448.3 - 138.6 \times (0.1614)^{1/2} + 193.1 \times 0.1614} = 0.1617 \ \text{g L}^{-1} \\ C_{i=5} &= \frac{192.00 - 0.80}{1448.3 - 138.6 \times (0.1617)^{1/2} + 193.1 \times 0.1617} = 0.1617 \ \text{g L}^{-1} \end{aligned} \qquad \text{(S2-7)}$$

S3 Experimental alabaster solubilities

Table S3-1. Experimental solubilities of alabaster compared with literature values of $CaSO_4 \cdot 2H_2O$

temperature °C	[NaCl] g kg^{-1} sln.	$C_{experimental}$ g L^{-1}	$C_{literature}$)[a] g L^{-1}	ratio
20.6	0	2.65	2.55	1.038
21.9	0	2.59	2.56	1.009
3.7	0	2.32	2.25	1.032
22.4	35.1	6.54	6.48	1.009
21.4	37.9	6.92	6.63	1.043
4.0	35.0	6.12	5.87	1.042

)[a] O'Brien et al. [1]

S4. Data summary of dissolution and permeation kinetics

Alabaster dissolution rates

Table S4-1. Experimental details of experiments to determine the mass transfer coefficients (k_w) of the water boundary layer, using alabaster dissolution rates. t = exposure time, Δm = alabaster mass loss, temp. = temperature, Δ = calculated recession of the alabaster surface due to dissolution (adopting an alabaster density of 2.3 g cm^{-3})

experimenter	stirring rate (min^{-1})	k_w (μm s^{-1})	t (h)	Δm (g)	temp. (°C)	Δ (mm)
4	0	3.0	18.6	0.59	21.7	0.20
4	0	2.8	7.0	0.24	22.6	0.08
4	0	2.3	5.0	0.13	22.6	0.04
4	0	2.5	4.8	0.14	21.8	0.05
2	90	6.4	8.5	0.57	20.8	0.20
2	200	11.0	5.3	0.61	20.1	0.21
2	200	11.8	5.0	0.62	21.1	0.21
1	200	12.2	21.6	1.82	19.5	0.63
2	400	17.7	3.3	0.61	20.3	0.21
2	400	19.5	3.1	0.62	20.5	0.21
1	400	17.8	25.2	2.28	20.2	0.79
2	600	24.4	2.6	0.65	20.4	0.22
2	600	27.8	2.2	0.64	21.0	0.22
1	600	27.3	6.5	1.45	20.0	0.50

Calcium sulphate permeation rates

Table S4-2. Experimental details of calcium sulphate permeation experiments. C_0 = estimated initial concentration in the donor compartment, mass balance = estimated C_0 relative to the concentration calculated from the spiked amount, k_o = overall mass transfer coefficient, temp. = temperature.

experimenter	stirring rate (RPM)	temp. (°C)	C_0 (g L^{-1})	mass balance (%)	k_o (μm s^{-1})	residual error (g L^{-1})
2	90	20.0	0.161	101	1.908 ± 0.011	0.0003
4	90	19.7	0.159	100	1.870 ± 0.006	0.0003
1	200	19.9	0.164	101	2.385 ± 0.004	0.0001
1	400	19.7	1.018	102	2.942 ± 0.024	0.0007
1	400	20.0	0.168	101	2.842 ± 0.009	0.0001
1	600	20.6	0.163	101	3.212 ± 0.004	0.0001

Atrazine permeation rates

Table S4-3. Experimental details of atrazine permeation experiments. C_0 = estimated initial concentration in the donor compartment, mass balance = estimated C_0 relative to the concentration calculated from the spiked amount, k_o = overall mass transfer coefficient, temp. = temperature.

experimenter	stirring rate (RPM)	temp. (°C)	C_0 (ng mL^{-1})	mass balance (%)	k_o (μm s^{-1})	residual error (ng mL^{-1})
1	90	22	34.5	90	1.54 ± 0.07	0.6
2	90	20	36.7	93	1.24 ± 0.04	0.7
2	200	20	34.0	85	1.62 ± 0.04	0.6
1	400		2.7	71	2.37 ± 0.24	0.1
1	400	22	33.6	88	1.92 ± 0.05	0.5
2	400	20	26.7	68	1.78 ± 0.14	1.0
1	600	23	31.7	83	2.36 ± 0.09	0.6
2	600	20	35.0	89	2.18 ± 0.10	0.9

S5. Mass transfer coefficients for alabaster dissolution under conditions of free convection

Churchill and Chu [2] showed that mass transfer rates for a vertical plate under conditions of free convection ($k_{w,free}$) can be modelled as

$$Sh = \frac{k_{w,free}\, L}{D_w} = 0.68 + \frac{0.670\, Ra^{1/4}}{\left[1+\left(\frac{0.492}{Sc}\right)^{9/16}\right]^{4/9}} \qquad \text{(S5-1)}$$

where $k_{w,free}$ is the mass transfer coefficient for free convection, L is the length of the plate, D_w is the diffusion coefficient of the solute, Ra is the Rayleigh number and Sc the Schmidt number

$$Sc = \frac{\nu}{D_w} \qquad \text{(S5-2)}$$

$$Ra = \frac{g L^3}{\nu D} \frac{\Delta\rho}{\rho} \qquad \text{(S5-3)}$$

where ν is the kinematic viscosity of the fluid, g is the acceleration of gravity, $\Delta\rho$ the density difference over the boundary layer, and ρ the density of the water.

Solvent and solute properties were evaluated at 22 °C (the temperature during the free-convection experiments), and $k_{w,free}$ was calculated from eq. S5-1 as follows.

Density of saturated (2.57 g L^{-1}) calcium sulphate solution [3]: ρ = 0.9999 g cm^{-3}

Density of water [4]: ρ = 0.9978 g cm^{-3}

Dynamic viscosity of water [5]: η = 0.9547 mPa s

Kinematic viscosity $\nu = \eta/\rho = 0.955 \cdot 10^{-6}$ m^2 s^{-1}

Diffusion coefficient of calcium sulphate was calculated by interpolation of logD_w vs. 1/T, using the salt diffusion coefficients from Li and Gregory [6], which yielded D_w = 847 μm^2 s^{-1}

The length of the plate was taken to be its surface area divided by its diameter: 12.6/4.0 = 3.1 cm

Inserting these values yields Sc = 1127, Ra = 7.6·10^8, Sh = 111, $k_{w,free}$=3.0 μm s^{-1}

S6. Model fit and residual errors of nonlinear least squares estimation

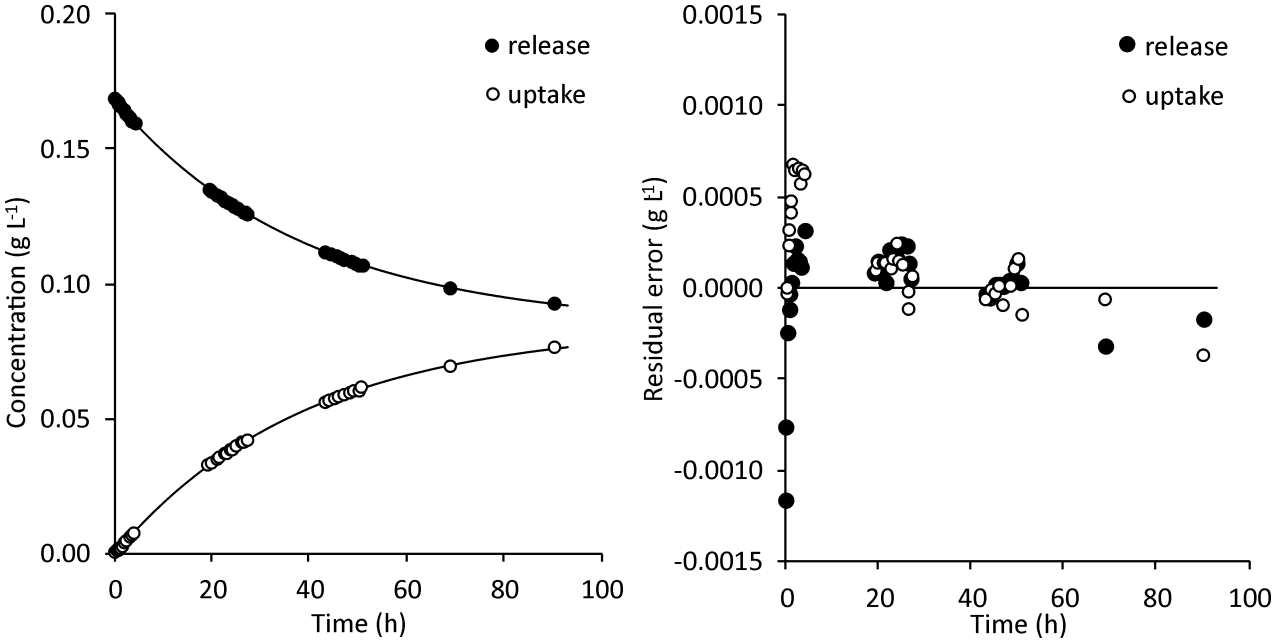

Figure S6-1. Results of the nonlinear least squares estimation using eqs. 10 and 11, using data from a calcium sulphate permeation experiment at 400 min^{-1}. Left panel: concentrations and model fit. Right panel: residual errors.

S7 Hydraulic permeation experiments

The difference in water height between the two compartments followed an exponential decrease with time, with a first order rate constant of 0.36 h^{-1}, in accordance with eq. 17 (Fig. S7-1). This rate constant corresponds to a hydraulic conductivity of K = 0.060 μm s^{-1}, and a membrane permeability of k =6.2·10^{-15} m^2 (eq. 16).

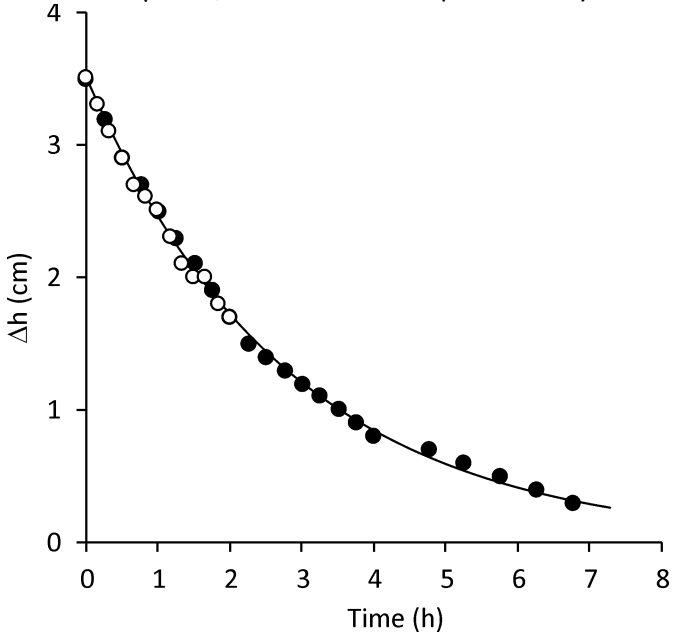

Figure S7-1. Difference in water height as a function of time in the diffusion cell, following the addition of 0.85 L water to one compartment and 1.20 L water to the other. The drawn line represents the model fit (eq. 17).

References

1. O'Brien DS, Booij K, Hawker DW, Mueller JF. 2011. Method for the in situ calibration of a passive phosphate sampler in estuarine and marine waters. *Environ. Sci. Technol.* 45:2871–2877.
2. Churchill SW, Chu HHS. 1975. Correlating equations for laminar and turbulent free convection from a vertical plate. *Int. J. Heat Mass Transf.* 18:1323–1329.
3. Millero FJ. 1972. The partial molal volumes of electrolytes in aqueous solutions. In Horne, RA, ed., *Water Aqueous Solut. Stucture Thermodyn. Transp. Process.* John Wiley and Sons, New York, pp 519–564.
4. Jones FE, Harris GL. 1992. ITS-90 density of water formulation for volumetric standards calibration. *J. Res. Natl. Inst. Stand. Technol.* 97:335–340.
5. Kestin J, Sokolov M, Wakeham WA. 1978. Viscosity of liquid water in range -8 ^{o}C to 150 ^{o}C. *J. Phys. Chem. Ref. Data*. 7:941–948.
6. Li Y-H, Gregory S. 1974. Diffusion of ions in sea water and in deep sea sediments. *Geochim. Cosmochim. Acta*. 38:703–714.